Canadian Journal of Physics

Research Article

Spectral features of photoionization of ground and excited levels of P I

Sultana N. Nahar

Department of Astronomy, The Ohio State University, Columbus, OH 43210, USA

Corresponding author: **Sultana N. Nahar** (email: nahar.1@osu.edu)

Abstract

Spectral features of photoionization of various fine structure levels of P I, (P I + hν → P II + e), are reported. These include characteristic features of Rydberg and Seaton resonances, equivalent electron levels, low and high lying excited levels, and their impact on the background cross sections, and effects of fine structure couplings. Calculations were carried out in the relativistic Breit–Pauli R-matrix method with close-coupling (CC) approximation that generates the resonances naturally. The CC wavefunction expansion for P I includes ground and 27 excited levels of the core ion P II with orbitals of $n = 3$ and $n = 4$ complexes and 87 configurations of P I for bound channel contributions. Photoionization cross sections (σ_{PI}) with detailed resonances are presented for all 543 fine structure levels of P I found with $1/2 \leq J \leq 15/2$ of even and odd parities and $n \leq 10$ and $l \leq 9$. The autoionizing resonances are delineated with a fine energy mesh to observe the fine structure effects. The ground level shows typical feature of smoothly decreasing σ_{PI} with increasing energy. However, a compressed set of narrow resonances is found to form by the coupling of channels in fine structure at the ionization threshold of photoionization for the ground and many excited levels. These resonances and strong Rydberg resonances in the low energy region are found in photoionization spectra of the five equivalent electron levels of P I. Low lying excited levels show presence of strong Rydberg resonances and many with enhanced background cross section. Prominent Seaton resonances due to photo-excitation-of-core, often with enhanced background, are seen in photoionization of single valence electron high lying excited levels. Partial cross sections of the ground level with various core ion states are also presented. The present results should provide high-accuracy parameters of various model applications, such as, for exoplanetary atmosphere spectroscopy.

Key words: photoionization spectra, spectral features, ground and excited states of P I, Breit–Pauli R-matrix method, Rydberg and Seaton resonances

1. Introduction

Phosphorus (P) is a biosignature element and is an essential component of DNA–RNA. It is a highly active element that forms compounds easily with other elements making it difficult to be seen in commonly observed spectra. See, for example, in Wikipedia [1]. It is abundant in the solar system, however, shows poor presence compared to other biogenic elements in astrophysical spectra making it one least studied element (e.g., ref. [2]). With sophisticated observatories, P is being observed more in the astrophysical spectra. With more exoplanets being discovered, search for existence of P, often considered as the clue of life, has risen [3]. Lines of P, if it exists, can be observed in the upper layer of the exoplanetary atmosphere. For spectral identifications and analysis it is essential to study the features and characteristics of phosphorus and its ions. P I is of particular interest because of its lines in the infrared region that can be detected by observatories such as James Webb Space Telescope.

Among the existent data available, energy levels of P I were measured by Martin et al. [4] and are available at the web based compilation table of National Institute of Standards and Technology (NIST) [5]. While Nahar and Shafique [6] report extensive set of transitions and lifetimes of P I, other available data include limited transitions at NIST compiled table calculated by Lawrence [7], Czyzak and Krueger [8], transitions and lifetimes calculated by Zatsarinny and Frose-Fischer [9] and Frose-Fischer [10], lifetimes measured by Curtis et al. [11] and Berzinish et al. [12].

Spectral features of all ionization stages of phosphorus were studied by Nahar and Shafique [6] using radiative transitions among levels. However, these spectral features can be modified by the process of photoionization. Photoionization cross sections include large number of narrow Rydberg resonances. Most of the resonances are dissolved by plasma density and enhance the background or the continuum of the spectrum. Strong and isolated resonances of photoionization can appear as absorption line spectra.

The objectives of the present work is to study photoionization of P I and spectral features with autoionizing (AI) resonances of ground and many excited levels using ab initio relativistic Breit–Pauli R-matrix (BPRM) method as adopted under the Opacity Project [13] and the Iron Project [14]. R-

matrix method is the most powerful method to study atomic processes to reveal the details of the process. Photoionization is different from radiative transitions between two levels for which oscillators strengths are obtained (e.g., ref. [6]). The present work is similar to use of R-matrix method for calculating photoionization cross sections of various atoms and ions such as iron ions [15]. Each atomic system has its own unique structure described by different wavefunctions and reveals features characterized by the atomic structure. Literature search indicates this is first detailed study of photoionization of P I.

2. Theory: Breit–Pauli R-matrix method

Details of the theoretical background for photoionization can be found, for example, in Pradhan and Nahar [16]. A summary description of the method is also given, for example, in Nahar et al. [15]. Hence, a brief theoretical outline is given here for the guidance of the methodology. Photoionization is a bound-free transition of an ion X^{+z} of charge z which can be direct as

$$h\nu + X^{+z} \rightarrow e + X^{++z} \tag{1}$$

Cross section for direct photoionization yields a smooth background that varies with energy. Photoionization can proceed through a two-step process with formation of an intermediate doubly excited state (indicated by double asterisks), known as the autoionizing (AI) state, as

$$h\nu + X^{+z} \leftrightarrow \left(X^{+z}\right)^{**} (AI) \leftrightarrow e + X^{++z} \tag{2}$$

For a neutral, such as the present case, initial charge is zero ($+z = 0$). This two-step process introduces a resonance in photoionization cross section. This process where a temporary quasi-bound state is formed with two excited electrons occurs most commonly in nature and is formed when the photon energy is equal to that of an AI Rydberg level,

$$E_{\rm R} = E_{\rm c}^{*} - z^2/\nu^2 \tag{3}$$

above the ionization threshold. $E_{\rm c}^{*}$ is an excitation energy of the core ion and ν is the effective quantum number of the outer electron with respect to $E_{\rm c}^{*}$. The AI state may autoionize into the continuum where the outer electron goes free, or undergo dielectronic recombination by emission of a photon. The AI resonance can be produced theoretically automatically by including the core excitation in the wave function expansion as considered in the close-coupling (CC) approximation.

The CC approximation treats the atomic system of $(N+1)$ electrons as a 'target' or the 'core' or the residual ion of N-electrons interacting with the $(N+1)$th electron. The total wave function, Ψ_E, of the $(N+1)$ electrons system in a symmetry $SL\pi(J\pi)$ is expressed by an expansion as (e.g., refs. [16, 17])

$$\Psi_E\,(e + \text{ion}) = A \sum_i \chi_i\,(\text{ion})\,\theta_i + \sum_j c_j \Phi_j \tag{4}$$

χ_i is the target or core ion N-electrons eigenfunction and θ_i is the $(N+1)$th electron function which can be in a bound or continuum state. The summation is over the ground and excited core ion states in the CC calculation. A is the antisymmetrization operator. The $(N+1)$th electron with kinetic energy k_i^2 corresponds to a channel labeled as $S_iL_i\pi_i k_i^2 \ell_i\,(SL\pi)$, where $S_iL_i\pi_i$ is the symmetry of the target state i. For $k_i^2 < 0$ the channel is closed and the Ψ_E represents a bound state, and for $k_i^2 > 0$ the channel is open and Ψ_E represents a continuum state. In the second sum, the Φ_js are bound channel functions of the $(N+1)$-electron system that account for short-range electron correlation, and subject to an orthogonality condition between the continuum and the bound electron spin-orbital functions. AI resonances are produced from interference effects among the closed and open channels.

In the relativistic BPRM method [14, 16] the Hamiltonian of the $(N+1)$-electron system is given by

$$H_{N+1}^{\rm BP} = \sum_{i=1}^{N+1} \left\{ -\nabla_i^2 - \frac{2Z}{r_i} + \sum_{j>i}^{N+1} \frac{2}{r_{ij}} \right\} + H_{N+1}^{\rm mass} + H_{N+1}^{\rm Dar} + H_{N+1}^{\rm so} \tag{5}$$

where the curly bracketed term is the nonrelativistic Hamiltonian and the additional terms are the relativistic one-body correction terms, the mass correction, $H^{\rm mass} = -\frac{\alpha^2}{4}\sum_i p_i^4$, Darwin, $H^{\rm Dar} = \frac{Z\alpha^2}{4}\sum_i \nabla^2\left(\frac{1}{r_i}\right)$, and the spin–orbit interaction, $H^{\rm so} = Z\alpha^2 \sum_i \frac{1}{r_i^3}\mathbf{l_i}.\mathbf{s_i}$, where p_i is the momentum of an electron, α is the fine structure constant, and $\mathbf{l_i}$, $\mathbf{s_i}$ are the orbital and spin angular momentum. Substitution of the CC wavefunction Ψ_E(e + ion) in the Schrodinger equation

$$H_{N+1}\Psi_E = E\Psi_E \tag{6}$$

results in a set of coupled equations that are solved using the R-matrix method [16–18, 19–21]. In R-matrix method the space is divided into two regions, inner and outer regions. Inner region is the sphere around the atomic system and includes effects of electron–electron correlations, short range potentials. The outer region extends from the boundary of the inner region out to infinity where the potential is mainly Coulombic. The BPRM method implements an intermediate coupling scheme where the set of $SL\pi$ terms in the wavefunction of (e + ion) system is recoupled for $SLJ\pi$ fine structure levels of the (e + ion) system. This is followed by diagonalization of the $(N+1)$-electron BP Hamiltonian. The solutions are either a continuum wavefunction Ψ_F for an electron with positive energies ($E \geqslant 0$), or a bound state wavefunction Ψ_B for negative total energies ($E < 0$).

With wavefunction expansions in the R-matrix formulation as given above, transition matrix element for photoionization is given by (e.g., ref. [16])

$$\left\langle \Psi_f \parallel \mathbf{D} \parallel \Psi_i \right\rangle \tag{7}$$

where Ψ_i and Ψ_f are the total wavefunctions of the initial and final states, $\mathbf{D} = \sum_i \mathbf{r}_i$ is the dipole operator representing the photon–ion interaction and the sum in $\mathbf{D}$ is over the number of active electrons. The generalized line strength $\mathbf{S}$ for the

Table 1. The table presents energy levels with their values (E_t) of core ion P II that were included in the wave function expansion of P I.

P II								
	Level		E_t(Ry) NIST	E_t(Ry) SS		Level		E_t(Ry) NIST	E_t(Ry) SS
1	$3s^23p^2(^3P_0)$		0.0	0.	15	$3s^23p4s\,(^3P^o_1)$	←	0.7905	0.8054
2	$3s^23p^2(^3P_1)$		0.0015	0.0020	16	$3s^23p4s\,(^3P^o_0)$		0.7939	0.8039
3	$3s^23p^2(^3P_2)$		0.0043	0.0056	17	$3s^23p3d\,(^3F^o_4)$		0.8001	0.8204
4	$3s^23p^2(^1D_2)$		0.0809	0.1051	18	$3s^23p3d\,(^3F^o_3)$		0.8016	0.8178
5	$3s^23p^2(^1S_0)$		0.1966	0.2135	19	$3s^23p3d\,(^3F^o_2)$		0.8037	0.8159
6	$3s3p^3\,(^5S^o_2)$		0.4164	0.3451	20	$3s^23p4s\,(^1P^o_1)$	←	0.8101	0.8211
7	$3s3p^3\,(^3D^o_3)$		0.5946	0.5915	21	$3s^23p4p(^1P_1)$		0.9262	1.0391
8	$3s3p^3\,(^3D^o_2)$		0.5948	0.5912	22	$3s^23p3d\,(^1P^o_1)$	←	0.9368	0.9603
9	$3s3p^3\,(^3D^o_1)$	←	0.5951	0.5910	23	$3s^23p3d\,(^3P^o_2)$		0.9443	0.9759
10	$3s3p^3\,(^3P^o_2)$		0.6995	0.7011	24	$3s^23p3d\,(^3P^o_1)$	←	0.9455	0.9774
11	$3s3p^3\,(^3P^o_1)$	←	0.7000	0.7016	25	$3s^23p3d\,(^3P^o_0)$		0.9472	0.9782
12	$3s3p^3\,(^3P^o_0)$		0.7001	0.7018	26	$3s^23p3d\,(^3D^o_1)$	←	0.9482	1.0043
13	$3s3p^3\,(^1D^o_2)$		0.7081	0.7328	27	$3s^23p3d\,(^3D^o_3)$		0.9482	1.0055
14	$3s^23p4s\,(^3P^o_2)$		0.7891	0.8096	28	$3s^23p3d\,(^3D^o_2)$		0.9487	1.0050

Note: They were obtained using code SUPERSTRUCTURE (SS) [25] using an optimized set of 12 configurations, $3s^23p^2(1)$, $3s3p^3(2)$, $3s^23p3d(3)$, $3s^23p4s(4)$, $3s^23p4p(5)$, $3s^23p4d(6)$, $3p^4(7)$, $3s3p^23d(8)$, $3s^23d^2(9)$, $3s^23d4s(10)$, $3p^34s(11)$, $3s3p3d^2(12)$, each with filled orbitals $1s^22s^22p^6$, and Thomas–Fermi scaling parameters for the orbitals λ_{nl}, 1.30 (1s), 1.25 (2s), 1.00 (2p), 1.18 (3s), 1.12 (3p), 1.2 (3d), 0.9 (4s), 0.80 (4p), 1.0 (4d). National Institute of Standards and Technology (NIST) energies [5] correspond to those of Martin et al. [4]. Arrows point to seven dipole allowed levels from the ground level where Seaton resonances form.

transition is obtained as

$$\mathbf{S} = \left|\langle \Psi_f \parallel \mathbf{D}_L \parallel \Psi_i \rangle\right|^2 = \left|\left\langle \psi_f \left| \sum_{j=1}^{N+1} r_j \right| \psi_i \right\rangle\right|^2 \tag{8}$$

where ψ_i and ψ_f are the initial and final state wavefunctions without the spin functions. Photoionization cross section (σ_{PI}) can be obtained from the line strength as

$$\sigma_{PI} = \frac{4\pi^2}{3c}\frac{E}{g_i}S \;\; [Mb] \tag{9}$$

where g_i is the statistical weight factor of the initial bound state, E is the incident photon energy, and cross section is in unit of Mega-barn, Mb.

The complex resonant structures in photoionization arise from couplings between open continuum channels ($k_i^2 \geq 0$) and closed channels ($k_i^2 < 0$) in the transition matrix at electron energies k_i^2 that correspond to AI states in Rydberg series $S_iL_iJ_i\pi_i\nu_i\ell_i$. To each core ion excitation belongs a series of AI resonances that are formed at the energies of its Rydberg states, E_R. However, the resonances are not single point lines in the σ_{PI}. Resonant and background shapes and features of photoionization form from the shape of the wavefunctions and how they interfere in the transition matrix. The shapes of resonances resemble to Lorentzian profile. Rydberg resonances are usually strong with high peaks when the excited level of the core ion that they belong to is dipole allowed from its ground level. Otherwise resonances are usually suppressed by the weak transition probability. The width of a resonance varies as $1/\nu^3$. Hence the width of a Rydberg resonance becomes narrower with increasing ν. The resonances have higher peaks and they become denser as they approach the excitation threshold of the core ion. With multielectron systems, identification of resonances become difficult due to overlapping of Rydberg series of resonances belonging to various excited thresholds.

3. Computations

BPRM computations are carried out using the R-matrix package of codes [20–23] which has several stages of computations, namely, STG1, STG2, RECUPD, STGH, STGB, STGF, PREBF, and STGBF. The calculation is initiated with STG1 by providing the wave function of the core ion as one initial input. We use the later version of code SUPERSTRUCTURE (SS) [24, 25] to obtain the core ion wave function. SS uses Thomas–Fermi–Dirac–Amaldi potential to represent electron–electron correlation interactions in central field approximation and includes relativistic contributions in Breit–Pauli approximation. STG2 and RECUPD carried out the angular algebra of the Hamiltonian, and STGH computed the Hamiltonian matrix and dipole transition matrices.

Wavefunction of P I included ground and 27 excited fine structure levels of the core ion P II, presented in Table 1. It is the same wavefunction used for the radiative transitions in P I [6]. Hence, present photoionization cross sections are self-consistent with oscillator strengths and other radiative data in ref. [6]. The optimized set of 12 configurations for the levels of P II, Thomas–Fermi scaling parameters (λ) for the orbitals, and comparison with observed energies of Martin et al. [4] available at NIST [5] are also presented in Table 1. As explained in ref. [6] that comparison shows agreement between SS and observed values is within a few percent mostly. For

Fig. 1. Top: Photoionization cross section σ_{PI} of the ground level, $3s^2 3p^3\left({}^4S^o_{3/2}\right)$, of P I showing typical spectral features of a ground level, a relatively smooth background that decreases with increase of energy. However, it shows presence of resonances at the ionization threshold of about 0.81 Ry. Bottom: Expanded features of the compressed resonances at the ionization threshold energy region of 0.810 to 0.815 Ry in σ_{PI} of the top panel. These features of resonances illustrate the coupling effect of fine structure channels. The resonances belong to the two excited levels $3s^2 3p^2({}^3P_{1,\,2})$ of the core ion, as shown by arrows in the figure, coupling with the ejected s and d electron in the continuum as explained in the text. The distinct features of the different series are easily visible.

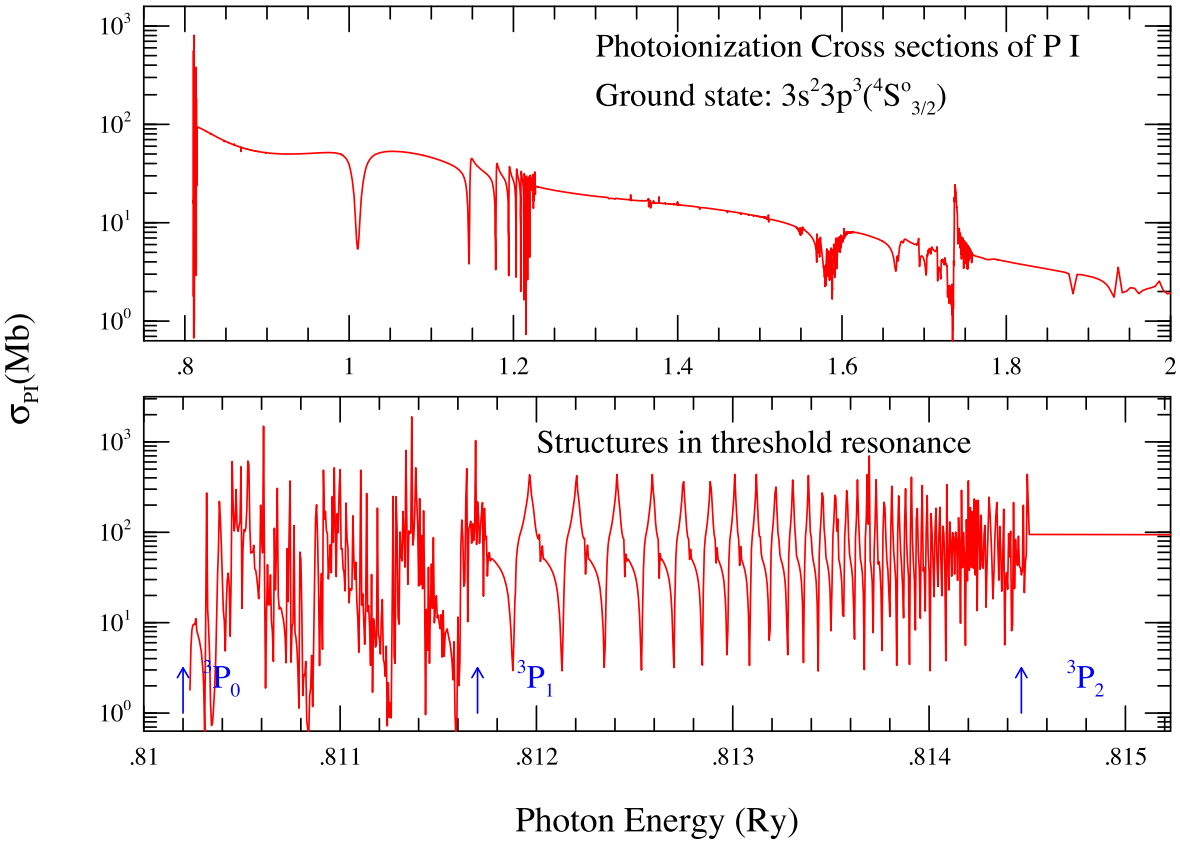

improved accuracy of energy positions of the resonances the calculated energies of P II were replaced by those available at NIST [5] during diagonalization of the $(N+1)$-electron Hamiltonian. Core ion excitation from the ground level to diople allowed levels introduce Seaton resonances (explained in the "Results and discussions section"). There are seven such transitions ($\Delta J = 1$ and change of parity) from the ground level of P II, $3s^2 3p^2({}^3P_0)$, which have been pointed by arrows for later reference.

The size of the wavefunction expansion was determined on the conditions of the convergence of resonances, first studied in detail in Nahar [26], Nahar and Pradhan [27], and Nahar [28]. As explained in these cited references, the convergence conditions typically depend on the strength of the core ion excitation. Hence resonant strengths are strong for strong dipole allowed transitions within the core ion. This strength is particularly highest for $\Delta n = 1$ core ion excitation. Beyond these core excitation the resonant strength starts to decay. The configurations of the excited core states in Table 1 indicate that the present wavefunction meet these criteria.

The R-matrix sphere was extended to 18 a_o in order to contain all short range interactions within it. The R-matrix basis for the orbitals was selected to have 20 terms. The final states of the $(N+1)$-electron system were determined from adding the angular momenta of core ion levels by the angular momenta of the outer electron, which ranges between $0 \leq l \leq 12$. They were used for fine structure levels with $1/2 \leq J \leq 15/2$. The second term of the wavefunction, eq. (3), included 87 configurations for P I.

STGB computed the bound states and energies of P I. Energy eigen values of the Hamiltonian matrix were obtained using fine energy meshes to search for the poles. BPRM codes do not identify the energy states. Spectroscopic identifications of the states were carried out, as described in ref. [6], using an algorithm based on quantum defect theory and angular algebra built in a code PRCBPID by Nahar [29, 30].

STGF computed the continuum wavefunctions which used a fine energy mesh in order to resolve the resonances. For each level, photoinization cross sections were computed for 10 000 energy points for 1 Rydberg of photo-electron en-

Fig. 2. Illustrating features of the four excited equivalent electron levels of the ground configurations (blue curves in top panels), $3s^2 3p^3 \left({}^2D^o_{3/2,5/2}\right)$ and $3s^2 3p^3 \left({}^2P^o_{3/2,1/2}\right)$, and three levels (red curves in the lower panels) of an excited configuration, $3s3p^4({}^4P_{1/2,\,3/2,\,5/2})$. Prominent resonances belong to the levels of $n = 3$ complex of the core ion. The arrows indicate highest core excitation for the prominent resonances.

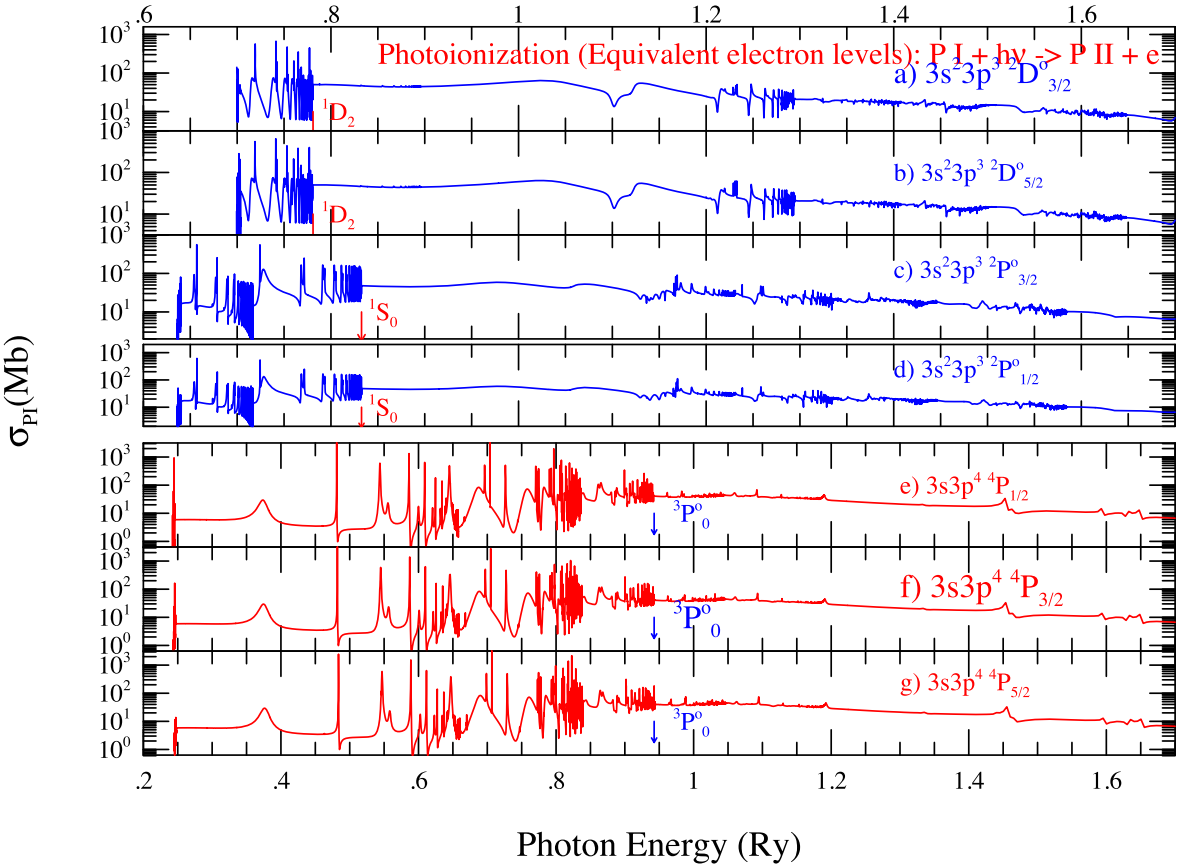

ergy. Low-energy resonances were resolved with a finer mesh. PREBF and STGBF were used to compute photoionization cross sections.

4. Results and discussions

We present detailed spectral features in photoionization of the ground and excited bound fine structure levels, 543 in total, with $1/2 \leq J \leq 15/2$ even and odd parities of $n \leq 10$ and $l \leq 9$ of P I. These energies and their accuracy are discussed in ref. [6]. The calculations were carried out in relativistic BPRM method using a CC wavefunction expansion that includes 28 levels of the core ion.

Photoionization features include Rydberg resonances formed by the quasi-bound AI states, Seaton resonances formed at dipole allowed excitation energies of the core ion, impact of the channel couplings in fine structure, shape of the background cross section, interference effects among them in photoionization cross sections σ_{PI}. All these features can be studied to find characteristics that are relevant to the states, such as ground and various types of excited states of P I. Convergence of resonances which indicates resonances becoming weaker with higher core ion excitation and are merging on the background cross section is used as a criteria for the wave function expansion and has been achieved. These features are illustrated below.

4.1. Photoionization of the ground level of P I and relativistic effects

Photoionization cross section (σ_{PI}) of the ground level of P I, $3s^2 3p^3 \left({}^4S^o_{3/2}\right)$, is presented in Fig. 1. The top panel shows total σ_{PI} of P I. The features are typical of a ground state photoionization where the background cross section is strong, smooth, and decreasing slowly with increase of energy. There are resonances appearing on the background but are weak for any significant contribution. Spectral features of the resonances depend on the shape and extension of the wavefunctions interacting in the transition matrix. Hence the ground level, for which the wavefunction is covering less space compared to other levels, typically shows prominent impact mainly from the low lying excitation of the core ion.

The compressed set of resonances right at the ionization threshold of about 0.81 Ry, as seen in Fig. 1, is not necessarily common. These compressed resonances, as expanded with high resolution in the lower panel, have formed through the coupling of fine structure channels, not allowed in LS coupling approximation. Following the selection rules, the

Fig. 3. Photoionization cross sections (σ_{PI}) of two low lying excited levels, (a) $3s^2 3p^2 4s(^4P_{5/2})$ and (b) $3s^2 3p^2 4s(^2D_{3/2})$, illustrating spectral features of these levels of P I with high peak Rydberg resonances and enhanced background cross sections at high energy region.

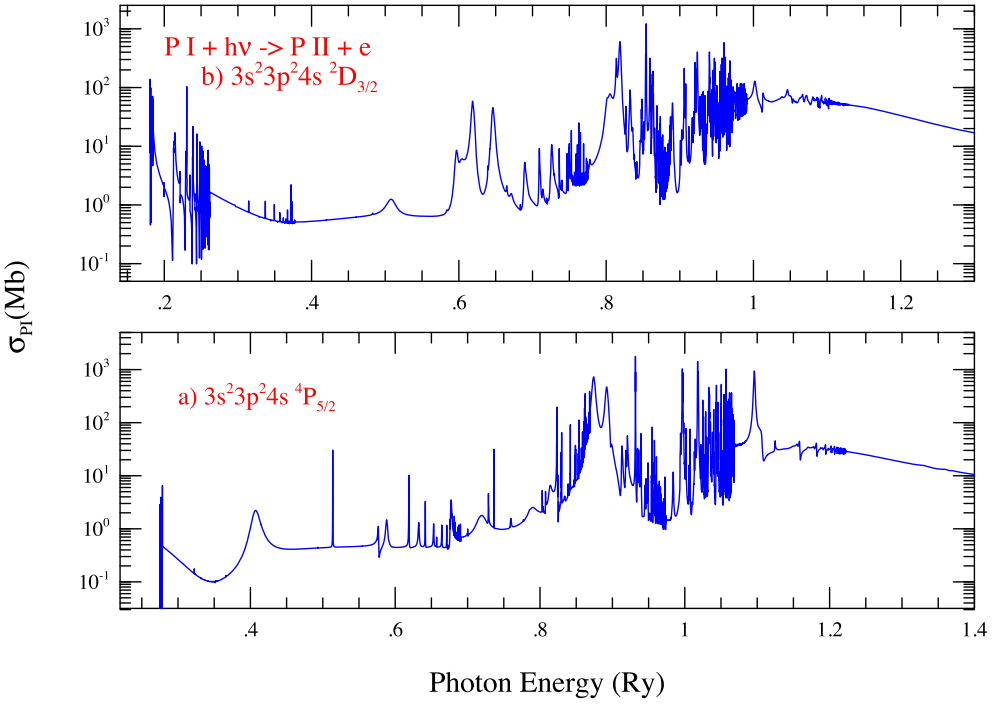

ground state of P I, $3s^2 3p^3\left(^4S^o_{3/2}\right)$ can photoionize to $J\pi = 1/2, 3/2, 5/2$ levels as a $3p$ electron is ejected out as an ϵs or ϵd electron in the continuum. The ground state of the core ion, P II, has three fine structure levels, $2s^2 2p^2(^3P_{0,1,2})$, where $^3P_0$ is the ground level and the other two are excited levels (positions shown in lower panel of Fig. 1). The s or the d electron can combine with the two excited levels of the core ion, $^3P_{1,2}$, to form $J\pi = 1/2.3/2, 5/2$ levels and introduce these Rydberg series of resonances $^3P_{(1,2)}\nu s$, νd, where ν is an effective quantum number. It may be noted that there are patterns of overlapping Rydberg series of resonances and that the patterns change at excited threshold energies as series converge to them.

Phosphorus with atomic number 15 is a relatively a small ion and has insignificant effects from relativistic fine structure. However, presence of resonances at and near ionization threshold energy due to couplings of fine structure channels not allowed in LS coupling, as explained above, has considerable impact on applications, such as, photoionization rates, electron–ion recombination at low temperature, plasma opacities etc. Fine structure splitting of a LS energy term of the core ion introduces a number of component excited energy levels resulting in increased number of Rydberg series of resonances forming from each component level. These resonances are more resolved than those from LS terms. While integration of resonances at high energy region will show little difference between use of relativistic and nonrelativistic approximations, the details of resonant features are more accurate with relativistic effects. Hence, use of BPRM approximation improves the accuracy in situations when details of resonances are important, such as, in high resolution measured features, near threshold resonances exist but can not be reproduced in LS coupling.

4.2. Photoionization of equivalent electron levels of P I

Most of the atomic systems have one or a few equivalent electron states where the outermost orbital contains more than one electron. Although a few, they are usually important contributors to applications, such as, for electron–ion recombination, photoionization rate, because of their strong resonances in the low energy region and slow decrease of the background cross sections with higher energy. The strong resonances can be seen in photoabsorption spectrum.

Figure 2 presents σ_{PI} of the seven equivalent electron levels of P I illustrating characteristic features in them. They are of the four excited levels (blue curves on the top panels) of the ground configuration, $3s^2 3p^3\left(^2D^o_{3/2,5/2}\right)$ and $3s^2 3p^3\left(^2P^o_{3/2,1/2}\right)$, and three levels (red curves in the lower panels) of the excited configuration, $3s3p^4(^4P_{1/2,3/2,5/2})$. These levels show that prominent resonances appear in the low energy region while those in the high energy region are weak and are merging on to the background cross sections. Prominent resonances belong to the low lying core ion excitation, up to $3s^2 3p^2(^1D_2)$ for P I levels $3s^2 3p^3\left(^2D^o_{3/2,5/2}\right)$, up to $3s^2 3p^2(^1S_0)$ for levels $3s^2 3p^3\left(^2P^o_{3/2,1/2}\right)$, and up to $3s3p^3\left(^3P^o_0\right)$ for levels $3s3p^4(^4P_{1/2,3/2,5/2})$ marked by arrows in the panels. It may be noted that all these core ion excitation for promi-

Fig. 4. Seaton resonances (positions are pointed by red arrows) in photoionization spectra of five excited levels, (*a*) $3s^23p^24p\left(^4S^o_{3/2}\right)$, (*b*) $3s^23p^23d(^2D_{3/2})$, (*c*) $3s^23p^25p\left(^2P^o_{1/2}\right)$, (*d*) $3s^23p^27p\left(^4P^o_{3/2}\right)$, and (*e*) $3s^23p^25d(^4D_{7/2})$ of P I demonstrating various characteristics as explained in the text.

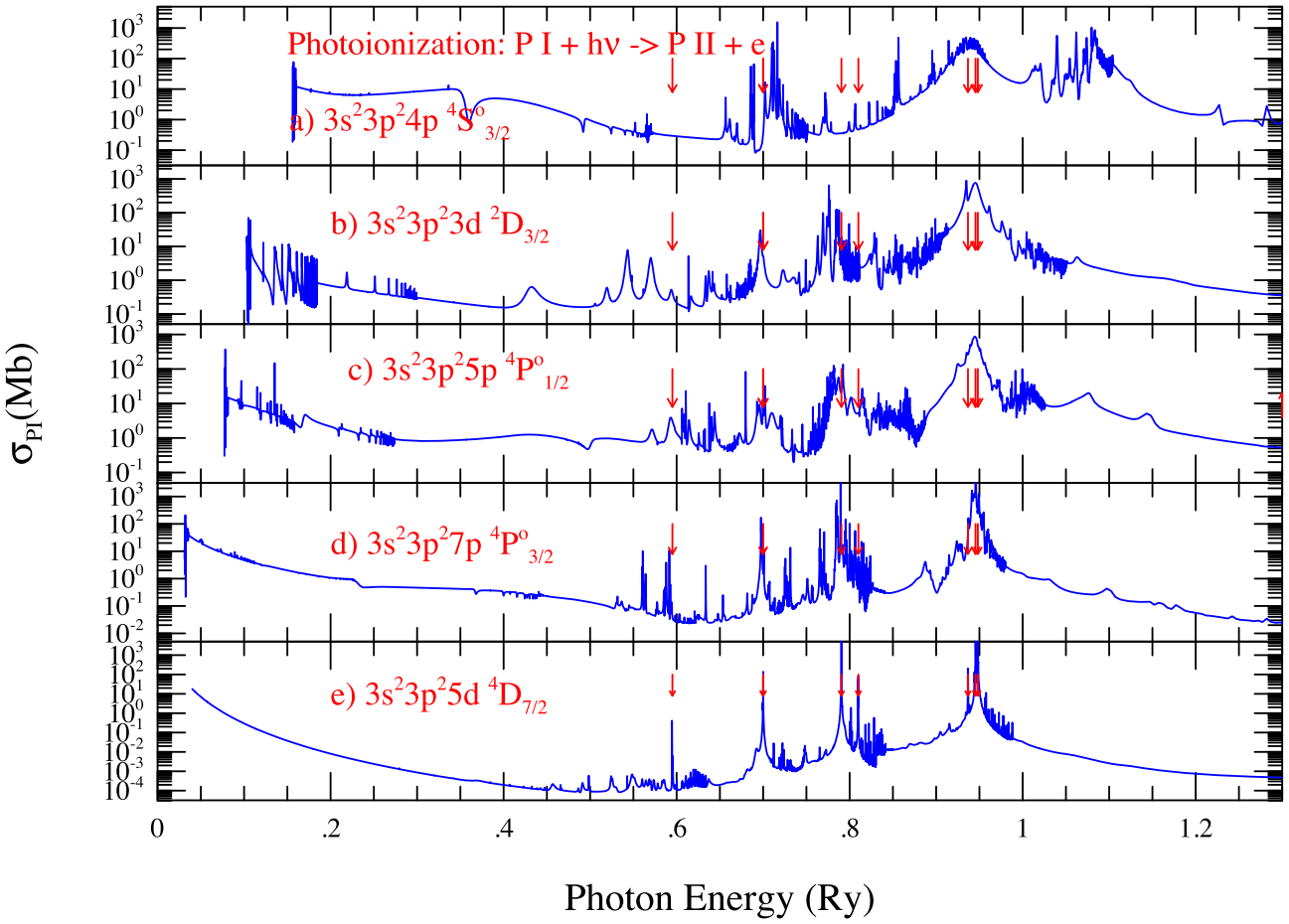

nent resonances belong to the $n = 3$ complex, that is, of the ground configuration of core ion P II. As explained above, the spectral features of the resonances depend on the shape and extent of the wavefunctions interacting in the transition matrix, equivalent electron levels which are typically low lying levels, show impact from the low lying excitation of the core ion.

4.3. Photoionization of low lying excited levels of P I

Low lying energy levels often display features of strong Rydberg resonances and interference effect on the background cross sections causing it enhance significantly.

Figure 3 presents photoionization cross sections (σ_{PI}) of two low lying excited levels, (a) $3s^23p^24s(^4P_{5/2})$ and (b) $3s^23p^24s(^2D_{3/2})$, of P I. Presence of compressed set of resonances at the ionization threshold is noted for both states. Strong Rydberg resonances appear from low to high energy regions. Strength and number of resonances depend on the core ion excitation they belong to and interference of overlapping series. Resonances belong to excitation that are dipole allowed for the ground level are stronger than others. The high energy resonances have led to enhanced background cross sections for both states. The resonances correspond to core ion excitation to both $n = 3$ and $n = 4$ states, but the change in features arising from $n = 3$ and $n = 4$ excitation is not distinctly visible. The reason is, as can be seen in Table 1, that $n = 3$ and $n = 4$ levels overlap, and hence causing overlap of their Rydberg series of resonances.

As photon energy continues to increase, resonances start to diminish. Diminishing resonances to smooth background at high energy beyond the highest core ion excitation included in the calculations indicate convergence of resonances.

4.4. Photoionization of high lying excited levels of P I and Seaton resonances

The high lying excited levels for which wavefunctions extend further away from the nucleus show prominent features of high lying core ion excitation. One main characteristic feature of photoionization of high lying excited levels with single valence electron is the presence of Seaton resonances. A Seaton resonance is introduced due to photo-excitation-of-core (PEC), that is, when the core ion goes through a dipole allowed excitation by its ground state while the outer electron remains as a spectator in an excited orbit before photoionization. The resonance can also appear, although not common,

Fig. 5. Partial photoionization cross sections of the gound level of P I leaving the core ion in the eight lowest levels of P II. Each partial cross section starts at the corresponding excitation thresholds of the core ion as specified in the panels.

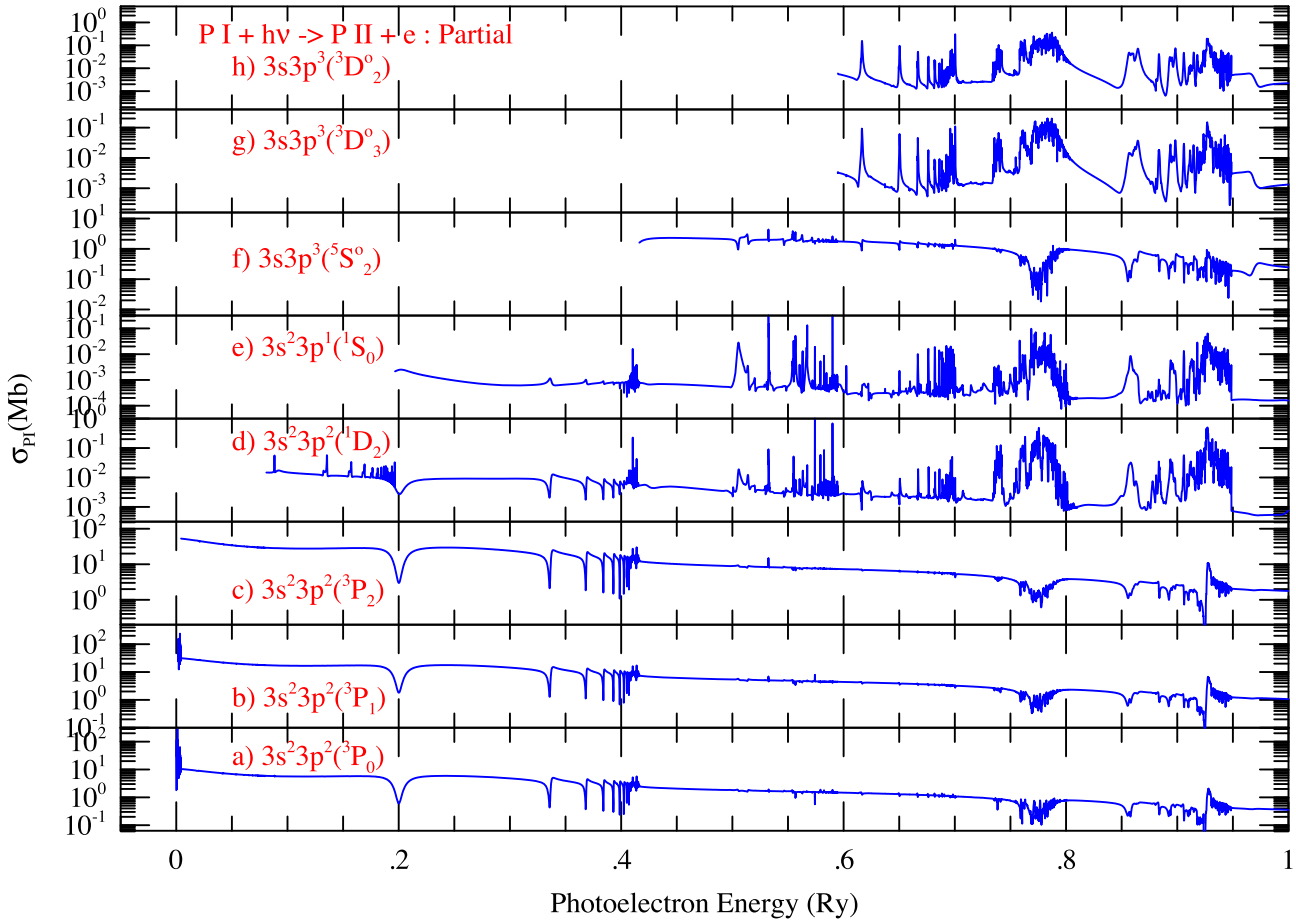

at a dipole allowed excitation threshold of a low-lying excited core level close to its ground level. PEC is manifested usually as a strong and wide Seaton resonance. There is no Seaton resonance for the ground level and equivalent electron levels. In contrast to a series of resonances, a Seaton resonance appears single at the excited energy of the core ion. Due to interference with Rydberg series of resonances, there could be a case when the peak of the broad feature of a Seaton resonance may not be located exactly at the excitation threshold energy but shifted slightly from it. High energy Seaton resonances are usually stronger due to higher transition probabilities than the lower ones.

Figure 4 presents Seaton resonances (positions are pointed by red arrows) in photoionization spectra of five excited levels, (a) $3s^23p^24p\left(^4S^o_{3/2}\right)$, (b) $3s^23p^23d(^2D_{3/2})$, (c) $3s^23p^25p\left(^2P^o_{1/2}\right)$, (d) $3s^23p^27p\left(^4P^o_{3/2}\right)$, and (e) $3s^23p^25d(^4D_{7/2})$ of P I. They are plotted in order of high to low ionization energy, which is basically lower to higher excited levels, as can be seen from the cross sections moving toward lower energy for photoionization. In each panel the positions of Seaton resonances remain the same as they correspond to excitation energies of the core ground level $^3P_0$ to various excited dipole allowed levels. The energy positions can be verified with the energies given in Table 1. This is different from Rydberg series of resonances which shift energies along with ionization energy.

Figure 4 shows that several Seaton resonances in the high energy region have enhanced background by orders of magnitude through interference with Rydberg resonances. This strong resonant feature of Seaton resonances in high energy photoionization of excited levels contribute significantly in various applications at high temperatures and contradicts the assumption of hydrogenic behavior of excited levels. Seaton resonances become more distinct with weakening Rydberg resonances with higher excited states. This is evident in the highest excited state photoionization (lowest panel) among the set of σ_{PI} in Fig. 4. However, this trend of Seaton resonances showing prominent presence does not continue as the excited levels move higher and at very high energy photoionization when Seaton resonances become weaker. We note that σ_{PI} is decreasing with higher photon energy indicating convergence.

4.5. Partial photoionization of P I leaving the core in various states

The total cross section is the sum of all partial cross sections that correspond to leaving the core ion in various states. For the present study for P I, we have considered core ion ex-

citation up to the 28th level. Hence, σ_{PI} of P I is the sum of partial cross sections leaving the core ion P II at 28 different levels. We present partial cross sections only for the ground level of P I. Partial cross sections leaving the core ion in ground and various excited levels are needed to calculate recombination rates for various recombiing levels, cascade matrix, etc. Figure 5 presents partial cross sections of the ground level of P I leaving P II in its first eight levels. Cross sections start at the ground and excitation thresholds of P II as specified in each panel. σ_P of leaving the core ion in various fine structure components belonging to an LS term has similar feature. As seen in the figure, cross sections in the first three lowest panels are similar since they correspond to leaving the core ion in the three levels, $^3P_{0,\,1,\,2}$, of term ^3P.

5. Conclusion

We present spectral features of photoionization of 543 fine structure levels of P I. These features have been categorized to four types of bound levels of P I - ground level, equivalent electron levels, low energy excited levels and high lying excited levels. The features can be described as (1) smooth background cross sections for the ground level with threshold resonances due to coupling of fine structure channels, (2) strong low-energy resonances for equivalent electron levels, (3) prominent Rydberg resonances with often enhanced background cross sections at high energy for low lying excited levels, and (4) prominent and often wide Seaton resonances with enhanced background for high lying excited levels. Impact of fine structure couplings is also demonstrated. Features of partial photoionization cross sections leaving the core ion in various excited thresholds are also illustrated. Similar BPRM calculations for spectral features of photoionization of P II [31] were reported earlier where features were benchmarked with the measured spectrum at Advanced Light Source of Berkeley Lawrence National laboratory.

Based on the BPRM methodology and similar work for other ions, accuracy of atomic data is expected to be 10%–15%. Hence they should provide precise model for astrophysical plasma, aimed at spectral analysis of exoplanetary atmosphere, and infrared observations, such as, from James Webb Space Telescope.

Acknowledgements

The author acknowledges use of high performance computers of Ohio Supercomputer Center for all computations of the present report.

Article information

History dates

Received: 2 June 2025
Accepted: 22 July 2025
Accepted manuscript online: 8 August 2025
Version of record online: 24 September 2025

Data availability

All atomic data will be available online at NORAD-Atomic-Data database at The Ohio State University [32].

Author information

Author ORCIDs

Sultana N. Nahar https://orcid.org/0000-0002-8750-3836

Author contributions

Conceptualization: SN
Data curation: SN
Formal analysis: SN
Funding acquisition: SN
Investigation: SN
Methodology: SN
Project administration: SN
Resources: SN
Software: SN
Supervision: SN
Validation: SN
Visualization: SN
Writing – original draft: SN
Writing – review & editing: SN

Competing interests

The author declares there are no competing interests.

References

1. Wikipedia: Available from https://en.wikipedia.org/wiki/Phosphorus
2. "OUR COSMIC SELVES", Sunday Opinion, NY Times, April 13, 2015.
3. N.R. Hinkel, H.E. Hartnett, and P.A. Young. APJ Lett. **900**, L38 (2020). doi:10.3847/2041-8213/abb3cb.
4. W.C. Martin, R. Zalubas, and A. Musgrove. J. Phys. Chem. Ref. Data, **14**, 751 (1985). doi:10.1063/1.555736.
5. National Institute of Standards and Technology (NIST) Gaithersburg, MD website: A. Kramida, Yu Ralchenko, and J. Reader, NIST ASD Team(2015), NIST Atomic Spectra Database (ver.5.3) . Available from http://physics.nist.gov/PhysRefData/ASD/levels_form.html
6. S.N. Nahar and B. Shafique. Can. J. Phys. **103**, 100 (2024). doi:10.1139/cjp-2023-0272.
7. G.M. Lawrence. Astrophys. J. **148**, 261 (1967). doi:10.1086/149143.
8. S.J. Czyzak and T.K. Krueger. Mon. Not. R. Astron. Soc. **126**, 177 (1963). doi:10.1093/mnras/126.2.177.
9. O. Zatsarinny and C. Forse-Fischer. J. Phys. B: At. Mol. Opt. Phys. **35**, 4669 (2002). doi:10.1088/0953-4075/35/22/309.
10. C. Forse-Fischer, G. Tachiev, and A. Irimia. Atom. Data Nucl. Data Tables, **92**, 607 (2006). doi:10.1016/j.adt.2006.03.001.
11. L.J. Curtis, I. Martinson, and R. Buchta. Phys. Scr. **3**, 197 (1971). doi:10.1088/0031-8949/3/5/001.
12. U. Berzinsh, S. Svanberg, and E. Biemont. Astron. Astrophys. **326**, 412 (1997).
13. The Opacity Project. Vol **1**, 1995, Vol. 2, 1996, Institute of Physics Publishing.
14. D.G. Hummer, K.A. Berrington, W. Eissner, A.K. Pradhan, H. E. Saraph, and J.A. Tully. Astron. Astrophys. **279**, 298 (1993).
15. S.N. Nahar, L. Zhao, W. Eissner, and A.K. Pradhan. J. Phys. B: At. Mol. Opt. Phys. **57**, 125002 (2024). doi:10.1088/1361-6455/ad4241.

16. A.K. Pradhan and S.N. Nahar. Atomic astrophysics and spectroscopy. Cambridge University Press, New York, 2011. doi:10.1017/CBO9780511975349.
17. M.J. Seaton. J. Phys. B, **20**, 6363 (1987). doi:10.1088/0022-3700/20/23/026.
18. P.G. Burke. R-matrix theory of atomic collisions. Springer. 2011. doi:10.1007/978-3-642-15931-2.
19. P.G. Burke and W.D. Robb. Adv. At. Mol. Phys. **11**, 143 (1975). doi:10.1016/S0065-2199(08)60030-5.
20. K.A. Berrington, P.G. Burke, K. Butler, M.J. Seaton, P.J. Storey, K.T. Taylor, and Y. Yan. J. Phys. B, **20**, 6379 (1987). doi:10.1088/0022-3700/20/23/027.
21. K.A. Berrington, W. Eissner, and P.H. Norrington. Comp. Phys. Commun. **92**, 290 (1995). doi:10.1016/0010-4655(95)00123-8.
22. S.N. Nahar and A.K. Pradhan, J. Phys. B, **27**, 429 (1994). doi:10.1088/0953-4075/27/3/010.
23. H.L. Zhang, S.N. Nahar, and A.K. Pradhan. J. Phys. B, **32**, 1459 (1999). doi:10.1088/0953-4075/32/6/010.
24. W. Eissner, M. Jones, and H. Nussbaumer. Comp. Phys. Commun. **8**, 270 (1974). doi:10.1016/0010-4655(74)90019-8.
25. S.N. Nahar, W. Eissner, G.X. Chen, and A.K. Pradhan. Astron. Astrophys. **487**, 789 (2003). doi:10.1051/0004-6361:20030945.
26. S.N. Nahar. Phys. Rev. A, **58**, 3766 (1998). doi:10.1103/PhysRevA.58.3766.
27. S.N. Nahar and A.K. Pradhan. Phys. Rev. Lett. **116**, 235003 (2016). doi:10.1103/PhysRevLett.116.235003.
28. S.N. Nahar. Astron. Soc. Pacific Conf. Ser. **515**, 103 (2018).
29. S.N. Nahar and A.K. Pradhan. Phys. Scr. **61**, 675 (2000). doi:10.1238/Physica.Regular.061a00675.
30. S N. Nahar. New Ast. **21**, 8 (2013). doi:10.1016/j.newast.2012.10.003.
31. S.N. Nahar, E.M. Hernández, L. Hernández, A. Antillón, A. Morales-Mori, O. González, A.M. Covington, K.C. Chartkunchand, D. Hanstorp, A.M. Juárez, and G. Hinojosa. JQSRT, **187**, 215 (2017). doi:10.1016/j.jqsrt.2016.09.013.
32. S.N. Nahar. Atoms, **8**, 68 (2020). (NORAD, Available from https://nora d.astronomy.osu.edu/). doi:10.3390/atoms8040068.